

X-Ray Observation of Venus with the INTEGRAL Telescope

Kent Barbey¹
Supervisor: Volodymyr Savchenko¹

¹LASTRO, School of Physics, Ecole Polytechnique Fédérale de Lausanne, Switzerland

Abstract

On April 22 and 24, 2022, Venus was observed with the JEM-X detector of the *INTEGRAL* space telescope. The observation performed yielded a discussed positive observation of the planet using three different modelling methods of the incoming flux of the source. All yielded a positive average flux at the 3σ level. No evidence of correlation between the solar and venusian flux variability was found. A very solar flare and CME direction locator was tested and its limits quickly found because of the limited FoV of the satellites contributing to these events' coordinates in the HEK database. This report suggests that the solar system planets can be studied using the available *INTEGRAL* data gathered over the last 19 years.

Keywords: scattering - X-ray emission processes - Planets: Venus - Sun: X-rays, gamma-rays - Satellite: *INTEGRAL*

Contents

Introduction	2
INTEGRAL telescope	2
JEM-X detector	2
ODA-API	3
HEASARC and <i>INTEGRAL</i> Science Window Data	4
X-ray emission of planets: the case of Venus	4
Observation, data analysis and methods	5
Data selection	5
Models and assumptions	8
Solar events	10
Results	12
Fluxes results	12
Concordance with solar flux variations	14
Solar events locations	15
Discussion	17
Conclusion	18
Annex A	19
22.04 sky plots	19
24.04 sky plots	20
Non constant flux assumption fits	20
Constant flux assumption fits	22
Annex B	24

Introduction

The Sun's activity in April 2022 increased drastically compared to earlier that year. Indeed, 12 out of the 50 strongest Earth directed solar flares of the year were detected in that only month¹. Moreover, 159 coronal mass ejections (CMEs) were detected by the LASCO instrument aboard SOHO in April 2022². This is a $\sim 79\%$ increase compared to the average of the 5 precedent months. Combined with an elongation of Venus near its maximal value of 47.8° , the observation conditions of this planet in the high-energy ranges were close to optimal. This report presents the approach used to recover the X-ray flux from a moving object, Venus, in the 3-10 keV energy range using the data from the JEM-X instrument aboard the *INTEGRAL* telescope. The values detected from Venus' position are then compared to the Sun's activity during that period.

This **Introduction** section first presents the telescope and instrument used. Then the data retrieving method using the *Online Data Analysis - Application Programming interface (ODA-API)* of *INTEGRAL* is described. The main channels of X-ray emission of planets are presented.

The **Observation, data analysis and methods** section shows the steps in the selection of the data, the criteria, assumptions and models used. This comprises how the solar events were obtained and analysed.

The **Results** section presents the results of the Venus fluxes using three different methods. The fluxes are then time wise compared with the solar fluxes. A solar event locator is presented using the Sunpy library.

Finally, the obtained results are thoroughly examined and interpreted in the **Discussion** section. The significance and implications of the findings are analysed. Furthermore, future research directions are proposed, highlighting potential avenues for further investigation.

Annex A provides additional figures on the models used. **Annex B** lists the different useful resources affiliated to this project.

INTEGRAL telescope

The INTErnational Gamma-RAY Laboratory (*INTEGRAL*), launched in 2002 on an elliptic orbit around Earth, is ESA's successor mission to the Cos-B and CGRO telescopes. For 19 years, it has been producing complete maps of the sky in the soft-gamma ray and X-ray sources (keV-MeV range) thanks to its four main instruments: IBIS imager (15 keV-10 MeV), SPI spectrometer (20 keV-8 MeV with a 2 keV spectral resolution at 1.33 MeV), JEM-X X-ray monitor and the OMC optical camera (V-band)[1].

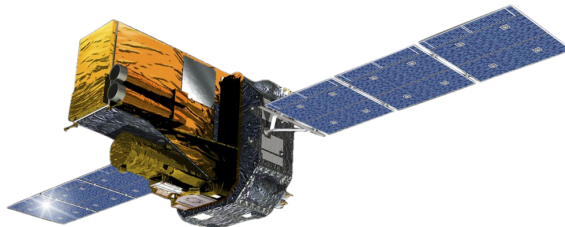


Figure 1: Artist's representation of the *INTEGRAL* telescope.

JEM-X detector

The Joint European Monitor for X-rays (JEM-X) is a complementary detector on-board the *INTEGRAL* telescope. It is primarily used to support the IBIS and SPI instruments in the lower energies for the studies of γ -ray and X-ray sources. It can however also provide independant scientific results for soft-spectra sources that could be serendipitously detected in the field-of-view(FOV) of the detector. This is the case for Venus here[2]. The characteristics of JEM-X can be found on Tab. 1. Fig. 2a shows a splitted view of the different constituents of the instrument. Fig. 2b is a top view representation of the coded mask of JEM-X. The instrument actually consists of two of these coded-aperture mask telescope units: JEM-X1 and JEM-X2. Each unit is composed of three parts: the detector, the electronics and the coded mask. For this study, only JEM-X2 data were used.

¹ <https://www.spaceweatherlive.com/en/solar-activity/top-50-solar-flares/year/2022.html>

² <https://www.sidc.be/cactus/catalog.php>

The detector of each JEM-X unit consists of a microstrip gas chamber (90% xenon and 10% methane at 1.5 bar). The incoming photons are absorbed in the xenon gas by photo-electric absorption and the resulting ionization cloud is then amplified in an avalanche of ionisations by the strong electric field near the microstrip anodes[2].

High-energy electromagnetic radiations cannot be observed using lenses or mirrors. Instead, patterns of materials opaque to the observed wavelengths called *coded-aperture masks* are used. An illustration is shown on Fig. 2b. By blocking the incoming radiation in a pre-determined pattern using mask elements, the image of the source observed casts a shadow on the detector. Reconstruction algorithms are then used to find the position of the source and its intensity³. The resolution of the mask is defined by the mask height above the detector and the mask element size. For JEM-X, these are respectively 3.4m and 3.3mm[2].

JEM-X Performance parameters	
Energy range [keV]	3 - 35
Detector area/effective [cm ²]	500/125
Energy resolution	1.3 keV @ 10 keV
Field-of-View (FoV)	4.8° (Fully coded)
Angular resolution (FWHM) [arcmin]	3
Pixel size [arcmin]	1.56

Table 1: JEM-X key performance parameters. See [here](#) for more details.

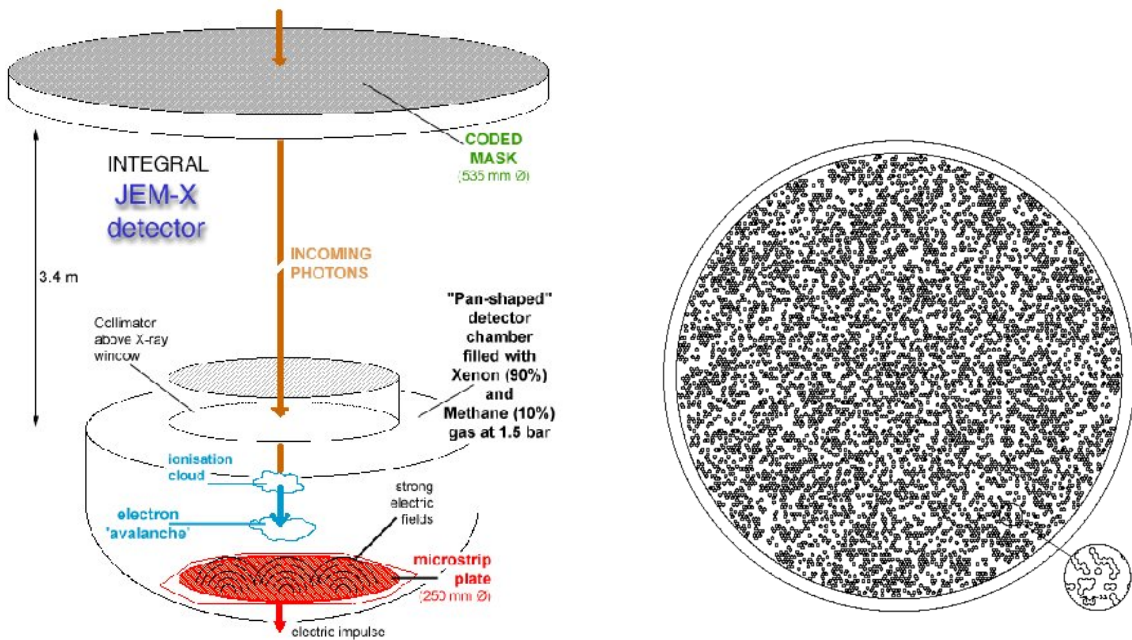


Figure 2: (left) Schematic diagram of the different JEM-X constituents. (right) JEM-X's coded mask.

ODA-API

Spanning more than nineteen years of nearly continuously taken data, the *INTEGRAL* archives contain information on a large number of sources. The mission was initially planned to operate only for five years and the data sets generated were supposed to stay relatively small[4]. But common to scientific space missions, the life of the telescope was extended as long as it stayed functional. The data analysis pipelines for all instruments uses the Offline Science Analysis (OSA) software distributed by the *INTEGRAL* Science Data Centre (ISDC). This software was optimised for the initial mission and the only solution for data processing before ODA-API was via a local installation of OSA on a user computer. Given the amount of data generated since then, the data processing resources now require a significant amount of computing resources. This is why the ODA was developed[4]. It provides an online *INTEGRAL* data analysis system using high-performance and cloud

³ See https://asd.gsfc.nasa.gov/archive/cai/coded_intr.html#section2 for details and [3]

computing technologies accessible through a web browser via the ODA website⁴ or through an API from e.g. a Jupyter notebook by querying the required parameters (see List. 1 for an example). The ODA-API was used in this study to retrieve the data from the *INTEGRAL* archives.

HEASARC and *INTEGRAL* Science Window Data

The High Energy Astrophysics Science Archive Research Center (HEASARC)⁵ is the primary archive for space missions studying high energy electromagnetic radiations phenomena. The *INTEGRAL* data is queried from the ISDC data servers using the `astroquery.heasarc` Python interface⁶.

INTEGRAL's activities are splitted into different categories called *windows*. *Science windows* (scw) are what interest us here. Quoting the ISDC, they are continuous time intervals during which all data acquired by the *INTEGRAL* instruments result from a specific spacecraft attitude orientation state. Scws have different parameters among which their observation identifier (Obs_ID) which is a sequence of 11 digits identifying each scw⁷.

X-ray emission of planets: the case of Venus

Most planets of our solar system emit in the X-ray domain by interacting with the solar wind(scattering). Most of them are known to shine in the < 3 keV domain. The main emission processes suspected to induce X-ray signal in planetary atmospheres are the following[5]:

1. Collisional excitation of neutral species and ions by charged particle impact (particularly electrons) followed by line emission.
2. Bremßtraslung emission due to electron collisions.
3. Solar photon scattering: elastic and K-shell fluorescent
4. Charge exchange of solar wind ions with neutrals
5. X-ray production from the charge exchange of energetic heavy ions with neutrals or by direct collisional excitation of ions.

See [5] for details about the different processes. Venus is a special planet for that matter as it is deprived of a protecting magnetic field. Studying such a planet is therefore valuable to understand the processes governing the solar wind and atmosphere interaction of planets. Moreover, comets are also deprived of a magnetic field and Venus therefore plays the role of an easily accessible model to understand the impact of the solar wind on these objects

Venus has already been observed in the < 3 keV domain notably for the first time with the Chandra telescope[6]. Venus was expected to be an X-ray emitter due to the verified presence of at least two processes: 3 and 5. In [6], the planet was clearly detected as a half-lit crescent exhibiting considerable brightening on the sunward limb. The data showed that the emission was dominated by O-K α , C-K α fluorescence and N-K α (0.28 keV, 0.53 keV and 0.40 keV). More importantly, the observed fluxes exhibited temporal variability on the scale of minutes. Since the solar flux can vary in a similar fashion, it was expected that these scattered solar X-rays would show the same variability. However the authors didn't find any time correlation between the two fluxes. They explained this result as being due to the fact that solar X-rays are predominantly emitted from localised regions and that Venus was seeing a 46.5°-48° rotated side of the Sun. The solar flux was measured from the GOES satellites orbiting Earth and not Venus. No charge-exchange interactions were measured at these energy ranges and none were expected given the sensitivity of the telescope.

To observe such charge exchange interactions, Venus was observed during and after it was hit by a powerful interplanetary coronal mass ejection (ICME) in [7]. Heavy ion flux up to 10 keV were observed that were due to charge-exchange interactions with the ICME.

See [5, 8] for a great deal of details on the interaction of the solar wind with Venus' atmosphere and solar system planets in general.

⁴ <https://www.astro.unige.ch/mmoda/>

⁵ <https://heasarc.gsfc.nasa.gov/>

⁶ <https://astroquery.readthedocs.io/en/latest/heasarc/heasarc.html#using-alternative-heasarc-servers>

⁷ See <https://heasarc.gsfc.nasa.gov/W3Browse/integral/intscw.html> for more details.

Observation, data analysis and methods

Data selection

Given that Venus was never purposely targeted by any of the *INTEGRAL* instruments, the idea was to scan the different science windows (scw) of the telescope corresponding to the planet's position in the sky at that moment. Many scw fulfil this condition. Given that planets emit mostly in the softer range of the X-ray spectra, only JEM-X data was used[5, 8]. To ensure the best data quality, other criteria were applied in the data selection. First, scw with increased sun activity were targeted. The sun regained activity following its 11 years cycle in 2021. The April and May 2022 months, with an increase in $\sim 79\%$ and 107% were appropriate. The elongation of Venus with respect to Earth and the telescope were also an important criteria. The elongation represents the Sun-Earth-Venus angle. When the angle is too small, Venus is by construction close to the Sun in the telescope's FoV and hence unobservable (and unobserved by the telescope anyway). **Fig. 3** illustrates the concept of elongation and **Fig. 4** shows Venus' position during the month of April 2022. The months of April and May 2022 also showed elongation angles close to the maximal value of 47.8° .

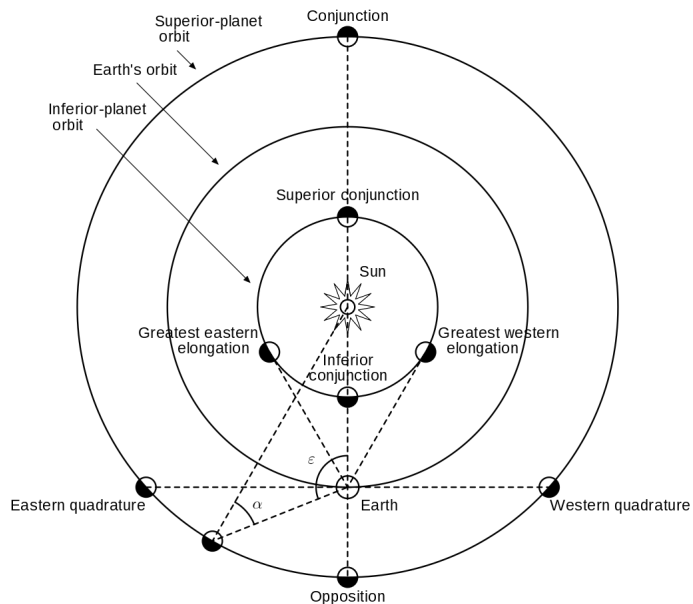


Figure 3: Heliocentric diagram of the positional representation of the Earth with respect to inner and outer planets. The greatest elongation is the α angle. It represents the Sun-Earth-Planet angle and is only shown for an outer planet on this diagram.

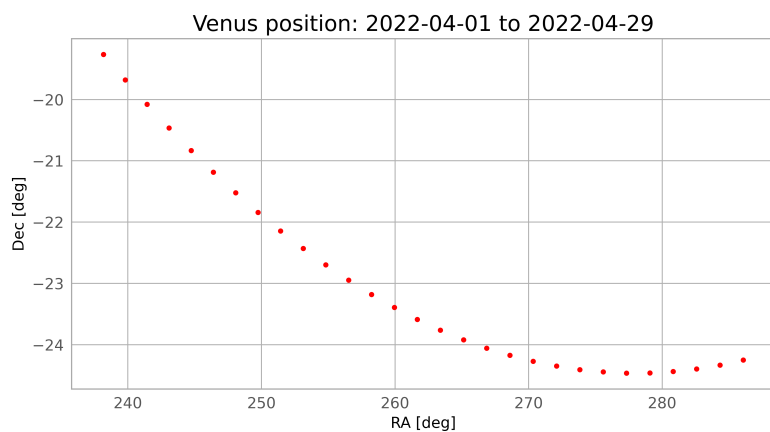


Figure 4: Position of Venus every day in the ICRF between the 01.04.2022 and 29.04.2022.

The query was made with the ODA-API given the criteria above and following the parameters listed below:

```

1   par_dict = {
2     "E1_keV": "3",
3     "E2_keV": "10",
4     "detection_threshold": "5",
5     "instrument": "jemx",
6     "osa_version": "OSA11.2",
7     "product": "jemx_image",
8     "product_type": "Real",
9     "scw_list": scw_list,
10    "integral_data_rights": "all-private",#all-private or public
11    "token": token
12  }
13

```

Listing 1: Query parameters template used for both dates.

Quoting [2]: *In practice, the transmission of the collimator beyond an off-axis angle of 5° is so low that only the very brightest sources can be observed at larger angles.* Therefore, all queries are made with a radius of maximum 5 degrees. The energies probed range from 3 keV to 10 keV. The scws observer identifiers are fed to the API for each date and the data is retrieved in the form of fits files.

The only scws satisfying these criteria were found in April 2022: four on the 18th, two on the 20th, fourteen on the 22nd and six on the 24th. The data of the 18th and the 20th were eventually not used due to Venus being too excentered in the image. Some scws from the 22nd and 24th were discarded for the same reasons. A summary of all final scws used is shown on **Tab. 2** as well as Venus' characteristics.

Date	scw_id	Time (UTC)	Elongation [°]	Apparent size ["]	Illumination [%]	Δ [AU]
22.04.2022	249400200010	04:12:03 - 04:45:23	43.88	17.89	64.30	0.93
	249400210010	04:47:45 - 05:20:55	43.88	17.89	64.31	0.93
	249400220010	05:22:52 - 05:56:13	43.88	17.89	64.32	0.93
	249400230010	05:58:34 - 06:31:43	43.87	17.88	64.33	0.93
	249400240010	06:33:55 - 07:07:14	43.87	17.88	64.34	0.93
	249400250010	07:09:37 - 07:42:45	43.87	17.88	64.34	0.93
	249400260010	07:44:42 - 08:18:03	43.85	17.87	64.35	0.93
	249400270010	08:20:27 - 08:53:35	43.85	17.87	64.36	0.93
	249400310010	10:41:30 - 11:14:50	43.85	17.87	64.37	0.93
	249400320010	11:17:16 - 11:50:21	43.84	17.87	64.37	0.94
	249400330010	11:52:20 - 12:25:41	43.84	17.86	64.38	0.94
24.04.2022	249500240010	19:47:17 - 20:20:27	43.50	17.52	65.33	0.95
	249500250010	20:22:48 - 20:55:58	43.49	17.51	65.34	0.95
	249500260010	20:58:10 - 21:31:29	43.49	17.51	65.35	0.95
	249500270010	21:33:27 - 22:06:47	43.48	17.50	65.36	0.95

Table 2: Journal of observations and parameters. scw_id: science window identifier, Δ: distance from INTEGRAL, Illumination: fraction of Venus illuminated as seen from observer computed at the beginning of each scw.

A noteworthy aspect of targeting an object such as a planet with this telescope is that it moves in the integrated image. Scws last usually between 20min and 1 hour and this is enough for Venus to move in the image of about 1 to 2 pixels.

22.04.2022 data

The April 22 data consists of eleven scws. **Fig. 5** shows the flux map for the first scw of the list shown on **Tab. 2**. The start and end positions of Venus are plotted. A strong source is plotted too using its coordinates retrieved from the SIMBAD server⁸ in order to check that Venus' position is plotted correctly since it isn't visually visible on the plot. All the other flux maps are presented in the **Annex A**. **Fig. 6** shows a mosaic done using all valid scws from the list with the ODA. All known strong gamma-ray and X-ray sources appearing in each scw are plotted.

⁸ <https://simbad.unistra.fr/simbad/>

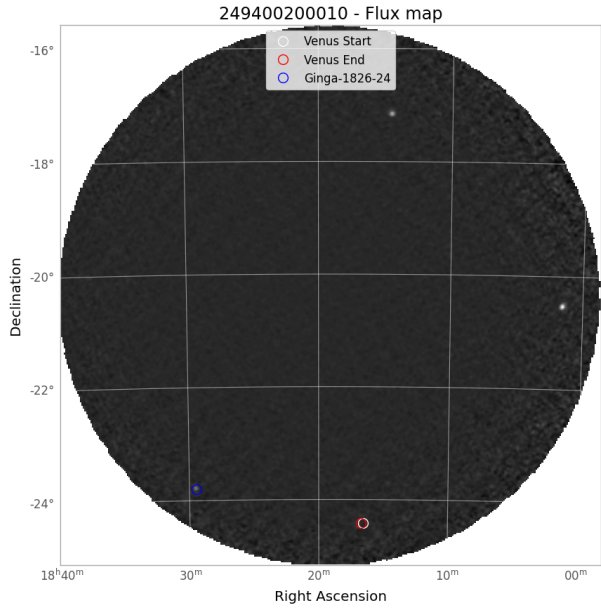


Figure 5: Flux map from the first scw where Venus is present on the 22.04.2022. The start and end positions of Venus are circled in white and red respectively. Another bright source is also plotted to verify the correct localisation approach. Here it is the X-ray binary Ginga 1826-24.

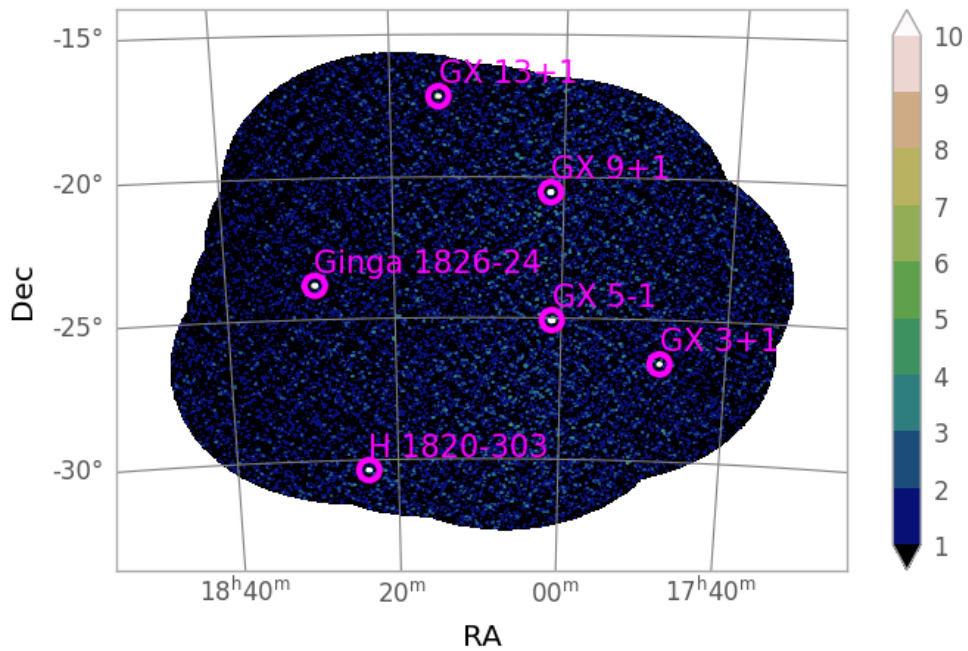


Figure 6: Mosaic made with the precedent images using the ODA plot tools for the 22.04.2022 data.

24.04.2022 data

The same process is done with the April 24 data which consists of four scws. **Fig. 7** shows the flux map for the first scw of the list shown on **Tab. 2**. All the other flux maps are presented in the **Annex A**. **Fig. 8** shows a mosaic done using all valid scws from the list with the ODA.

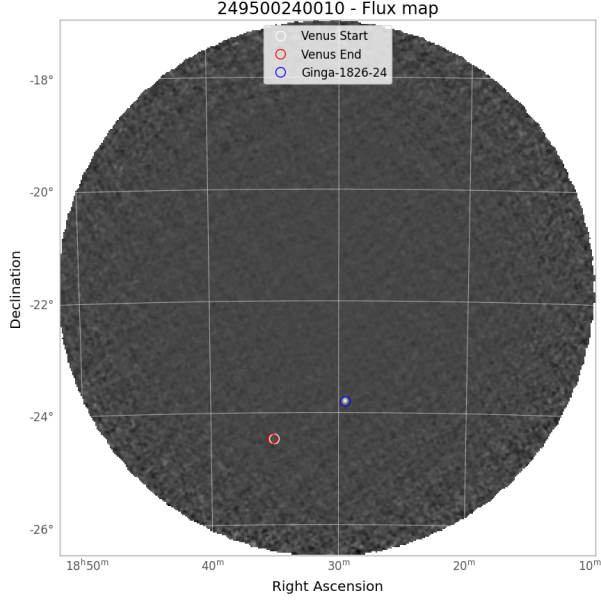


Figure 7: Flux map from the first scw where Venus is present on the 24.04.2022. The start and end positions of Venus are circled in white and red respectively. Another bright source is also plotted to verify the correct localisation approach. Here it is the X-ray binary Ginga 1826-24.

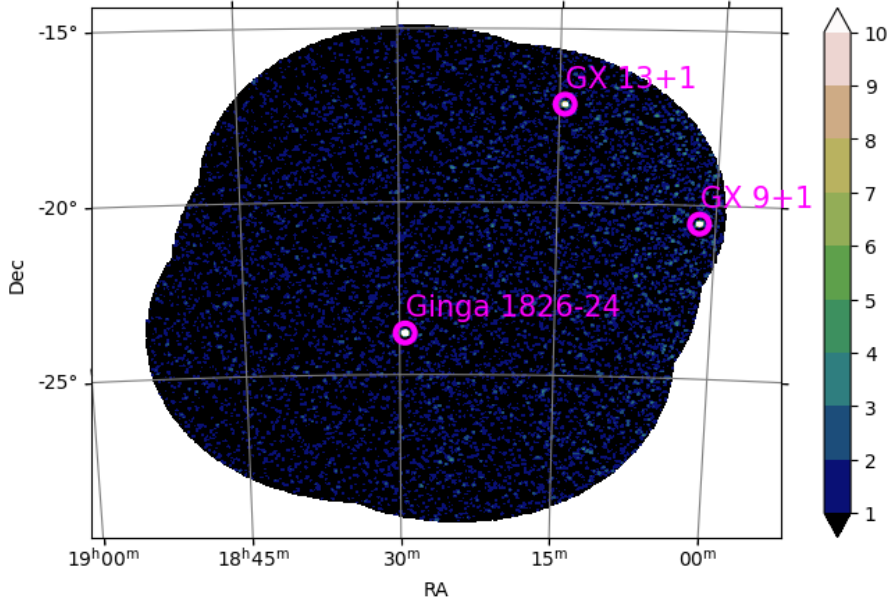


Figure 8: Mosaic of the 24.04.2022 data.

Models and assumptions

Three different models are used to retrieve the fluxes from Venus' position in the data arrays. The first idea is a really simple one: since Venus' apparent size is smaller than a pixel on the image, the idea is to take the value of the pixel Venus is in. This value can vary as Venus travels across the image. The uncertainty on the flux obtained is given by the square root of the value obtained for the same pixel in the variance map. The uncertainty is given at the 3σ -level representing a 99.7% confidence interval assuming a normal distribution of the possible values.

The second way of finding the flux emitted at Venus' position is to fit the sum of 2D Gaussian functions on the position of Venus. This function should represent the Point-Spread Function (PSF) of the JEM-X detector. The only free parameter optimised during the fit is the height of the Gaussian. The width is fixed by JEM-X's

resolution of 3' meaning that $\sigma_x = \sigma_y = 0.82$ pixel. The center of the Gaussian is given by the position of Venus at the time of measurement. Since the planet moves in the image, it is a sum of 2D Gaussians that is fitted where the number of summed elements is two for simplicity: one for the start position of Venus in the scw and for the end position. From there, two assumptions can be made concerning the parameters to optimise which are the heights of each summed 2D Gaussian: the flux of Venus can be assumed to be constant in the whole scw or it can also be assumed that the flux has a variability smaller than the scw time frame and then both summed Gaussians' heights are optimised. [6] actually finds that the temporal variability of Venus' flux in the soft X-rays has a temporal variability of minutes like the solar flux. It is therefore interesting to test both ideas.

The functions fitted are the following:

$$f(x, y) = h + h_1 e^{-\left(\frac{(x-x_0)^2}{2\sigma_x^2} + \frac{(y-y_0)^2}{2\sigma_y^2}\right)} + h_2 e^{-\left(\frac{(x-x_0)^2}{2\sigma_x^2} + \frac{(y-y_0)^2}{2\sigma_y^2}\right)}, \quad (1)$$

where $h_1 = h_2$ is the constant flux assumption and $h_1 \neq h_2$ in the other case. The minimisation of the objective function is done using the `minimize` function of the `scipy` library. **Fig. 9** and **10** show respectively the constant and non constant flux assumptions models

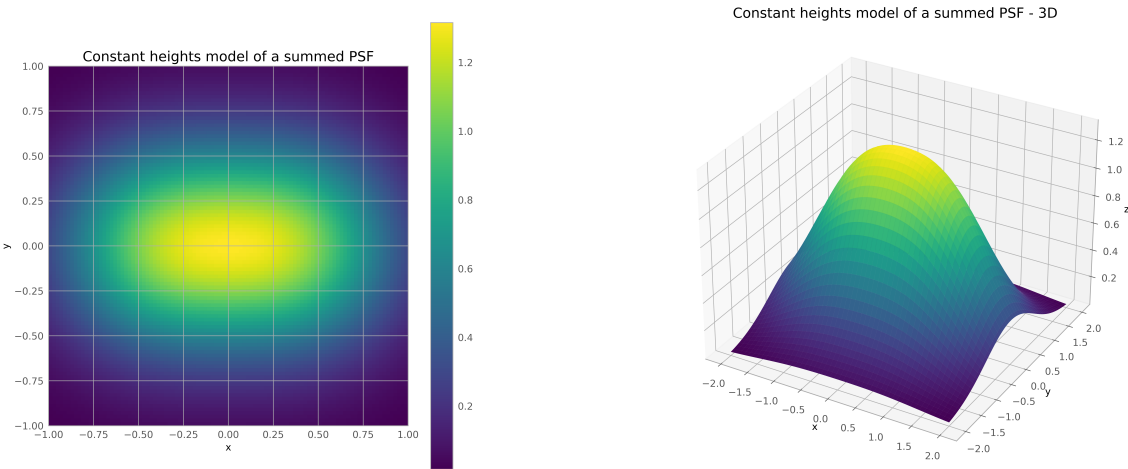


Figure 9: Constant summed PSFs used as models for Venus' flux.

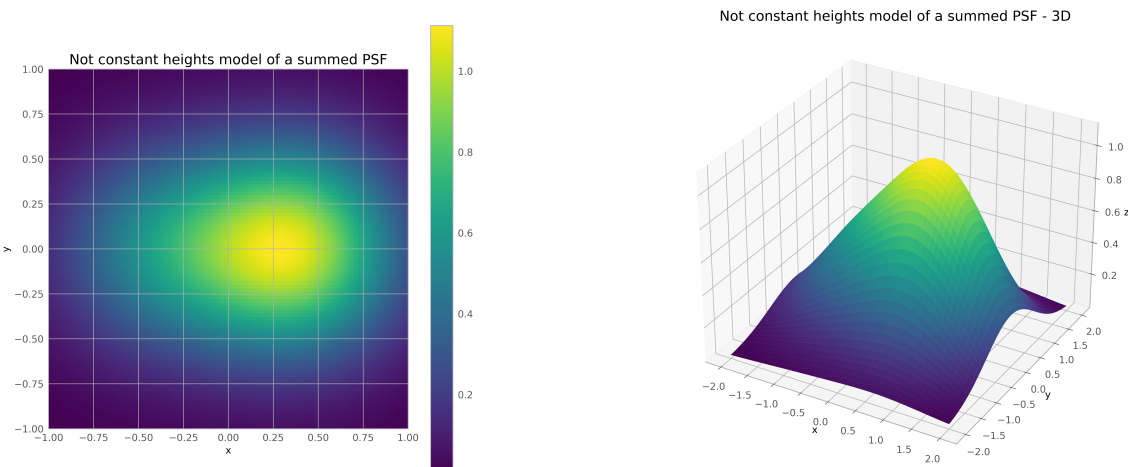


Figure 10: Non constant summed PSFs used as models for Venus' flux.

The uncertainty on the optimised height can be obtained in different ways. One is obviously MC sampling. The simpler way used here is to compute the relative deviations from the best-fitted height when scanning the heights around the optimised value gotten from the minimisation process. The deviations D are computed as follows from the residuals $r_i = (\text{data} - \text{fitted model})$ of each pixel i in a cropped square of 20 pixels centered on the start position of Venus:

$$\chi^2 = \sum_i r_i^2, \quad (2)$$

$$D = \frac{\chi^2 - \chi_{\text{best fit}}^2}{\chi_{\text{best fit}}^2} \quad (3)$$

The deviation threshold is set at 2%. The uncertainty on each point is then obtained by finding the interval when intersecting the $D(\text{height})$ function with an horizontal line representing the 2% threshold. The deviations for each point of the 22.04 scws are shown on **Fig. 11**. The same is done for the 24.04 scws.

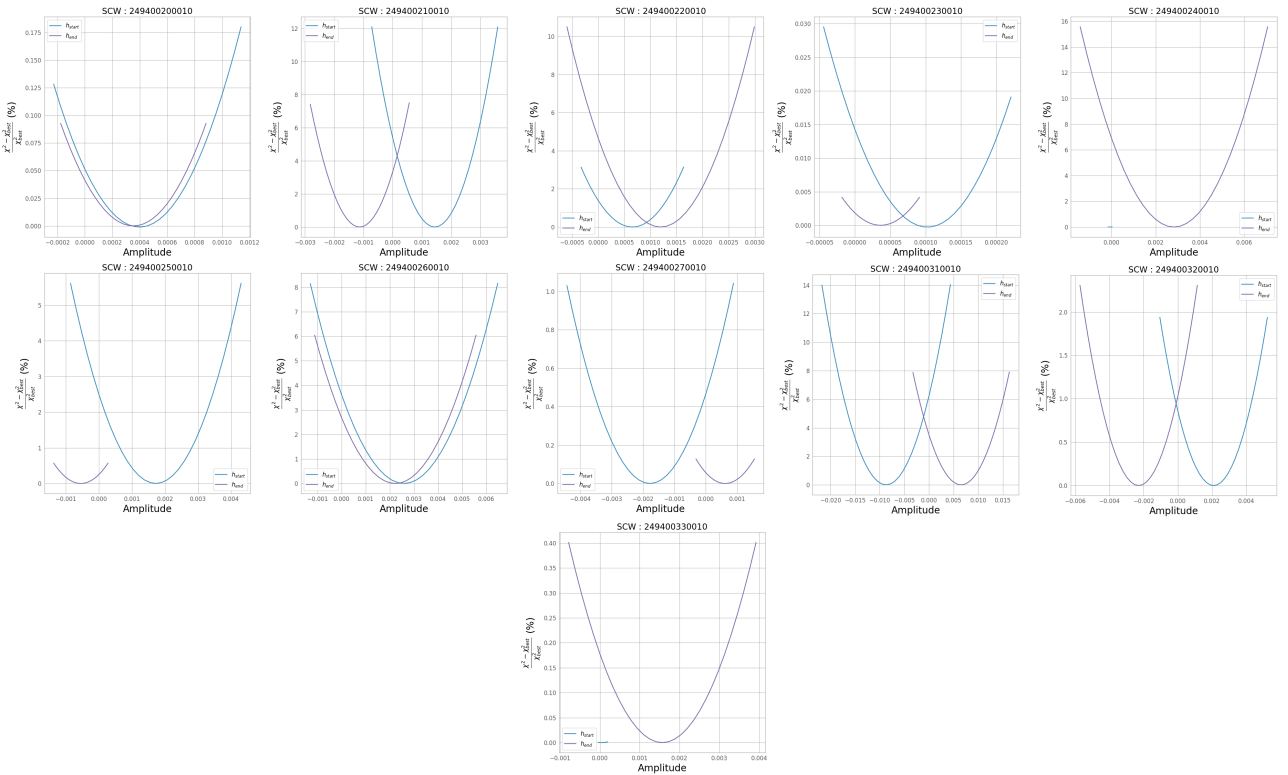


Figure 11: Normalised deviations from the optimised height for each flux point. The threshold is set at 2% of the best-fit value.

Solar events

The GOES spacecrafts are a series of geostationary meteorological satellites orbiting the Earth and providing information on space weather too. The GOES-16 satellite, currently in operation, monitors the solar X-ray flux in two different channels: XRSA (1-8 Å) and XRSB (0.5-4 Å).

The XRSA channel corresponding to energies ranging from 1.5 keV to 12.4 keV is used here. The solar flux in this channel for every day between the 19.04.2022 and 24.04.2022 is shown on **Fig. 12**.

The GOES satellites also monitor solar flares and classes them automatically. The CME are mostly monitored by other space telescopes such as SOHO via the LASCO detector. All these events are archived in the [Heliosphere Knowledge Database](#) (HEK) accessible through the Sunpy library. The surface coordinates of the events are given in the Helioprojective coordinate system (HPC). In order to find the direction of each event in the solar system, a transformation has to be made to the Heliographic Stonyhurst frame (HGS). The Sunpy library contains built-in functions enabling these transformations from the ICRF to HGS and HPC to HGS. **Fig. 13** illustrates the different coordinate systems in the Astropy and Sunpy packages.

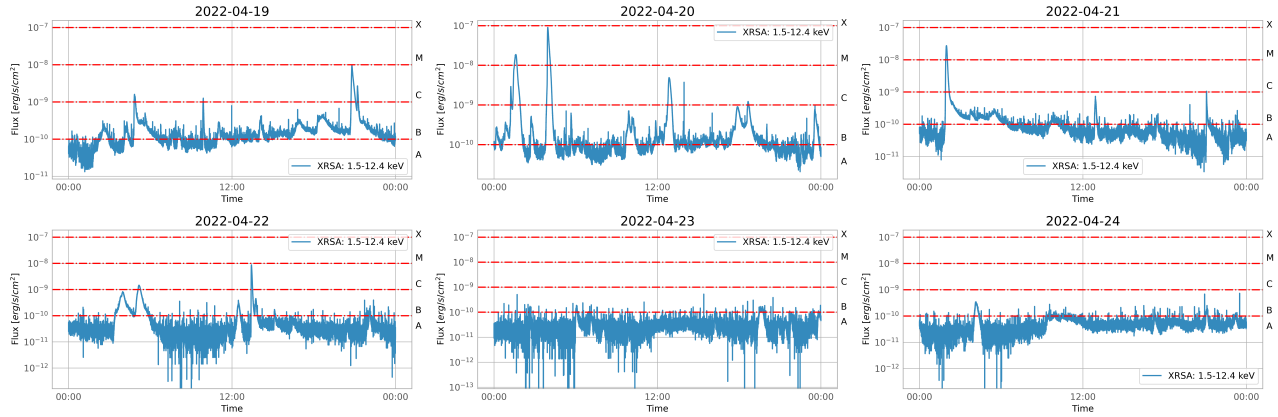


Figure 12: Solar flux in the XRSA channel(1.5-12.4 keV) of the GOES-16 spacecraft from the 19.04.2022 to the 24.04.2022. The solar flare classes are delimited on the right of each plot.

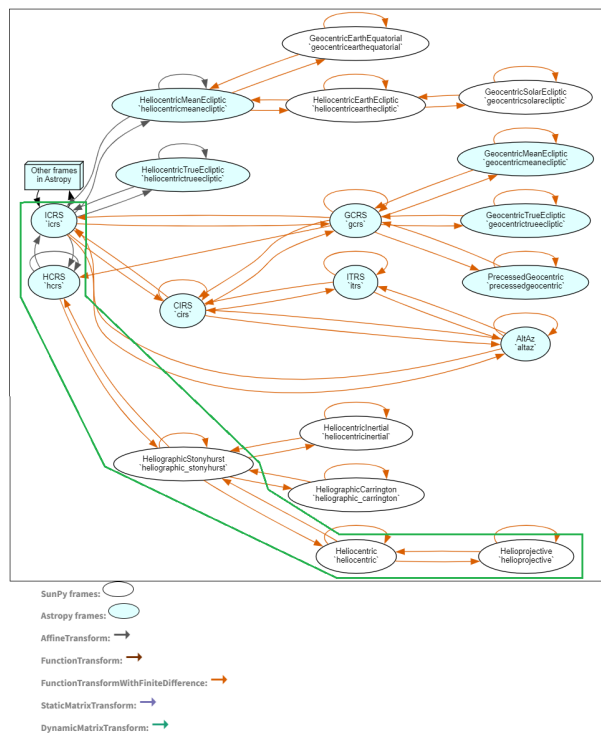


Figure 13: *Sunpy* and *Astropy* coordinate frames transformations. The path used for this study is boxed in green.

Results

The results are separated in three sections. First the fluxes from the three different methods are presented. Then, a comparison is made with the Chandra spectra from [6] and with the solar flux variation for the observation window. Finally, the solar event locator is presented.

Fluxes results

22.04.2022

Fig. 14 shows the flux obtained with the different methods for the 22.04.2022. The colours of the different data points correspond to the different scws listed in **Tab. 2** in that same order. As one wishes to combine the measurement of the fluxes with differing errors, a weighted average and uncertainty are computed in the following way:

$$\mu = \frac{\sum_i \frac{x_i}{\sigma_i^2}}{\sum_i \frac{1}{\sigma_i^2}} \quad (4)$$

$$\sigma(\mu) = \frac{1}{\sum_i \frac{1}{\sigma_i^2}} \quad (5)$$

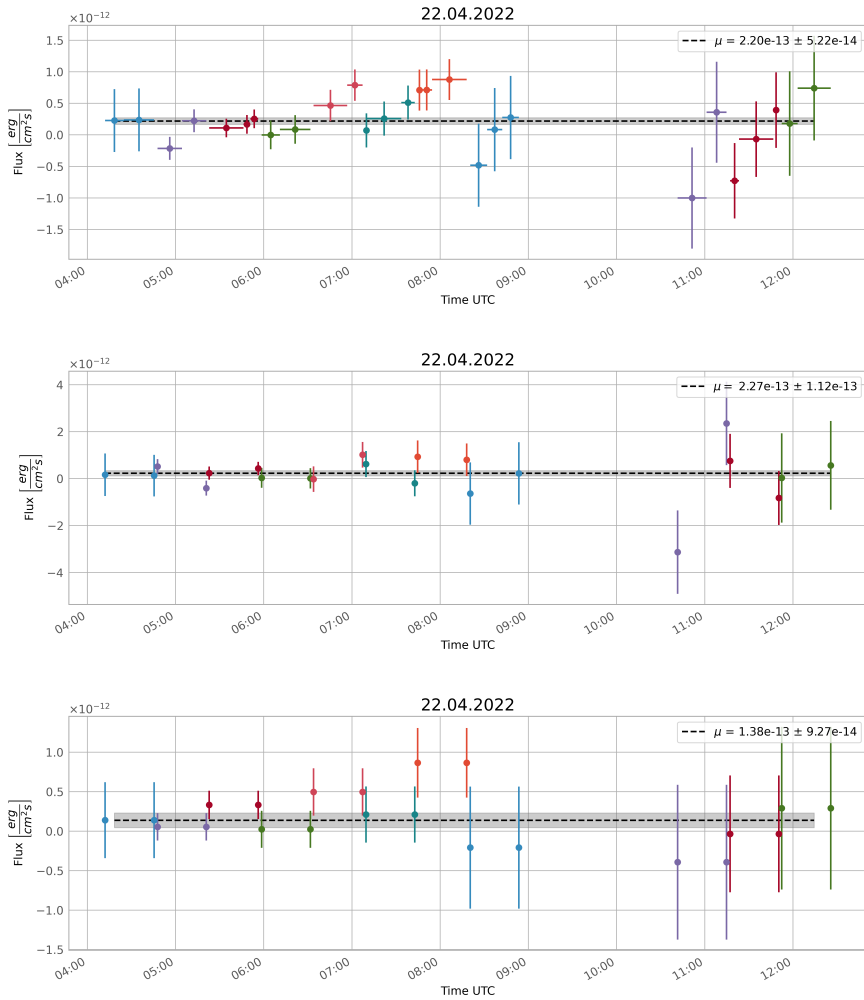


Figure 14: For the 22.04.2022, from top to bottom: LC using the pixel value, the non constant PSF model and the constant PSF model.

24.04.2022 The same is done with the 24.04 scws and is shown on **Fig. 15**.

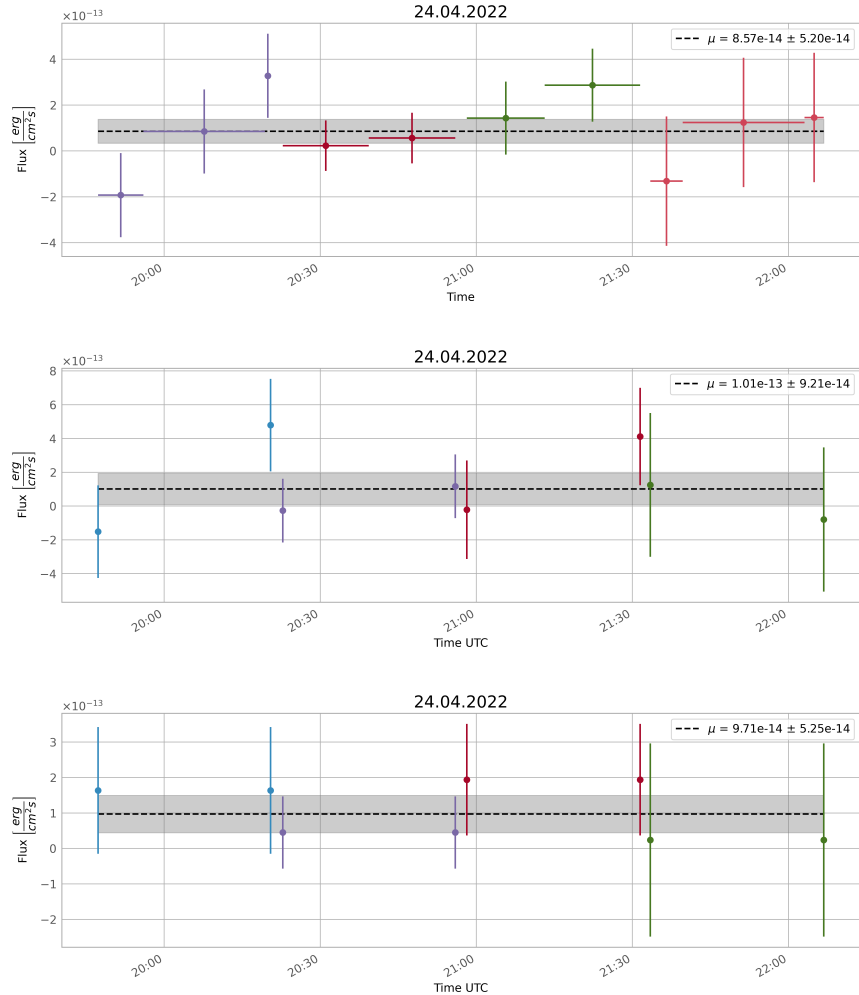


Figure 15: For the 24.04.2022, from top to bottom: LC using the pixel value, the non constant PSF model and the constant PSF model.

The average fluxes obtained with the first method for both windows are positive at the 3σ level as per how JEM-X's variance map is built. For the other two methods, the fluxes are also positive given the 2% threshold. Moreover, the values obtained between the three different methods are similar and reinforces the idea of a positive average flux observed in both windows.

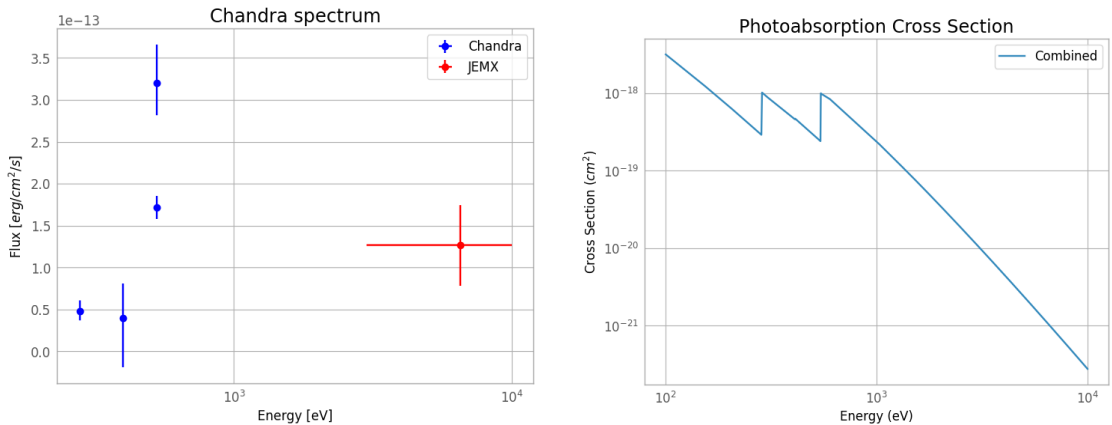


Figure 16: (left) Comparison between the flux values obtained in [6] and this study. (right) Cross-section model for the Venusian atmosphere using the `Xraydb.sqlite` database.

A comparison is made between the fluxes obtained in the [6] paper and here. The cross-section for fluorescence would suggest that the flux at higher energies should decrease. However, this is not the case here as shown on Fig. 16. This would suggest mainly two things: either the numbers are wrong in a way and do not represent correctly the flux from Venus or there are other physical sources apart from fluorescence that would contribute to Venus' luminosity in these higher energy ranges. For example, charge exchange interactions which could be more present in higher activity periods of the Sun[5].

Concordance with solar flux variations

Given that the Sun's flux variability is of the order of minutes and that it is the main X-ray emitting cause on Venus, it is interesting to compare its time variability with Venus' which also varies on a timescale of minutes[6]. The GOES-16 solar flux at 1 A.U. in the XRSA channel is shown at the top of Fig. 17 and 18. The time of each scw is plotted using the same colour code as before on these graphs.

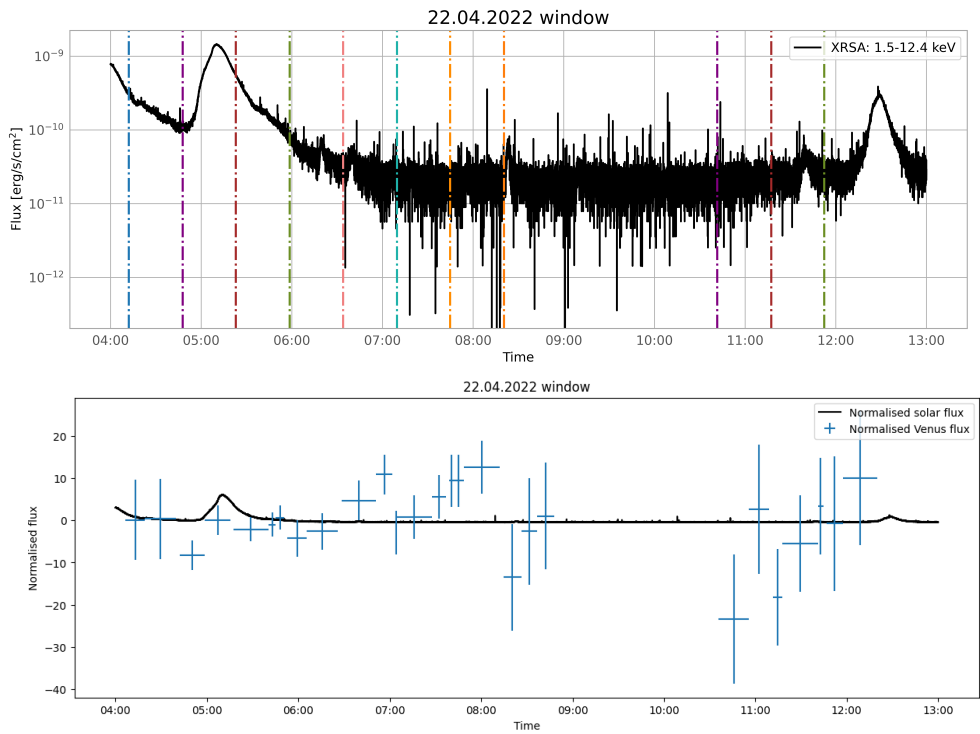


Figure 17: Top: 22.04.2022 scws restricted view of the solar flux in the XRSA channel of GOES-16 overplotted with the times of the LC points. Bottom: Normalised solar and Venus fluxes plotted together. The data point times were corrected from light travel.

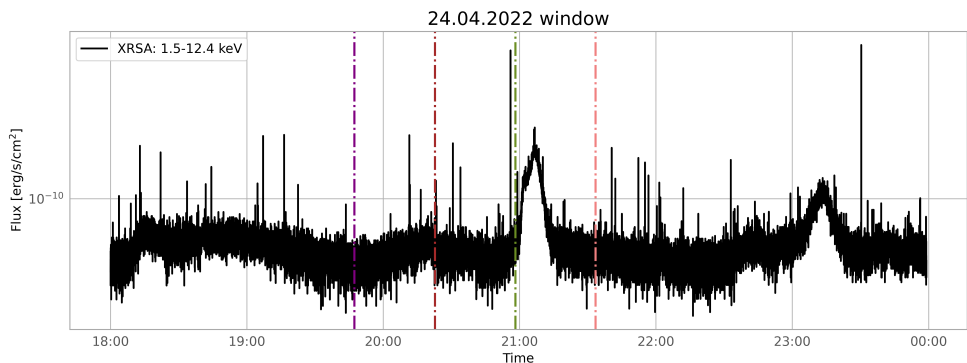
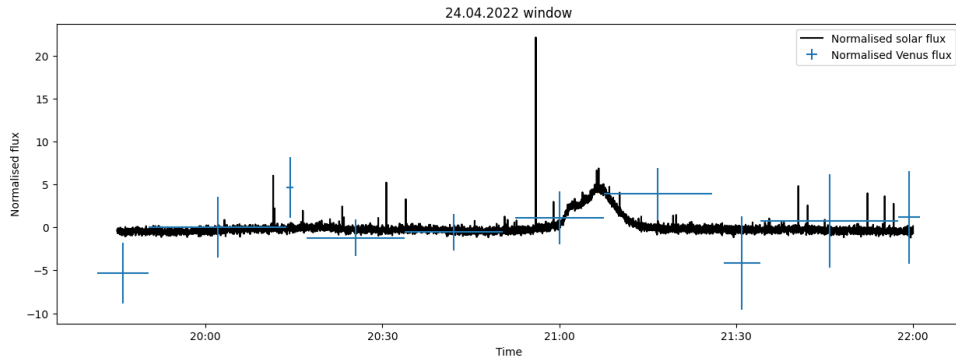


Figure 18: Top: 24.04.2022 scws restricted view of the solar flux in the XRSA channel of GOES-16 overplotted with the times of the LC points.



(continued) Bottom: Normalised solar and Venus fluxes plotted together. The data point times were corrected from light travel.

Moreover, Venus flux and the solar flux are normalised and plotted together on the bottom side of Fig. 17 and 18. The idea here is to inspect the time correlation between both quantities. The data points were corrected from light travel time. For the solar flux, the path is: Sun → Earth. For the Venus flux, it is: Sun → Venus → Earth. The data points are 5.6 minutes late on the solar flux data. A two-sample Kolmogorov-Smirnov test is performed on these sample. The significance level is set at a standard 5%. The results are p-values of 2.6% and 4.8% for respectively the 22.04.2022 and the 24.04.2022 windows.

The estimated average energy deposited on Venus in X-ray from the first scw to the last for each day and for the three different methods is given by:

$$E = \frac{\pi r_{\oplus}^2 \mu \Delta t}{\text{illumination}}, \quad (6)$$

where r_{\oplus} is Venus' radius and Δt is the duration from the first scw to the last on one of the two days observed. The results are the following:

Method/Date	22.04.2022	24.04.2022
Duration [s]	29618	8370
Pixel value [10^{16} erg]	1.15 ± 0.27	0.13 ± 0.077
Constant PSF [10^{16} erg]	0.72 ± 0.14	0.14 ± 0.077
Non-constant PSF [10^{16} erg]	1.18 ± 0.58	0.15 ± 0.13

Table 3: Estimated energy deposited on Venus given the three flux methods.

The results all overlapped except for the 22.04.2022 window with the constant PSF method.

Solar events locations

The direction of propagation of the solar flares and CMEs are estimated in the HGS thanks to the HEK data based on the HPC coordinates given by the GOES satellite for the flares and the LASCO instrument on SOHO for the CMEs. The model is as simplistic as it can get but it is a first try at such as estimation. A line is drawn between the centre of the Sun and the surface coordinates of the event. The results are shown on Fig. 19. The events' directions are clearly biased and this is discussed in the next section.

Fig. 20 shows an image of the M1.1 class flare detected as the first peak on the 22.04.2022 solar flux plot on Fig. 17 by the AIA imager.

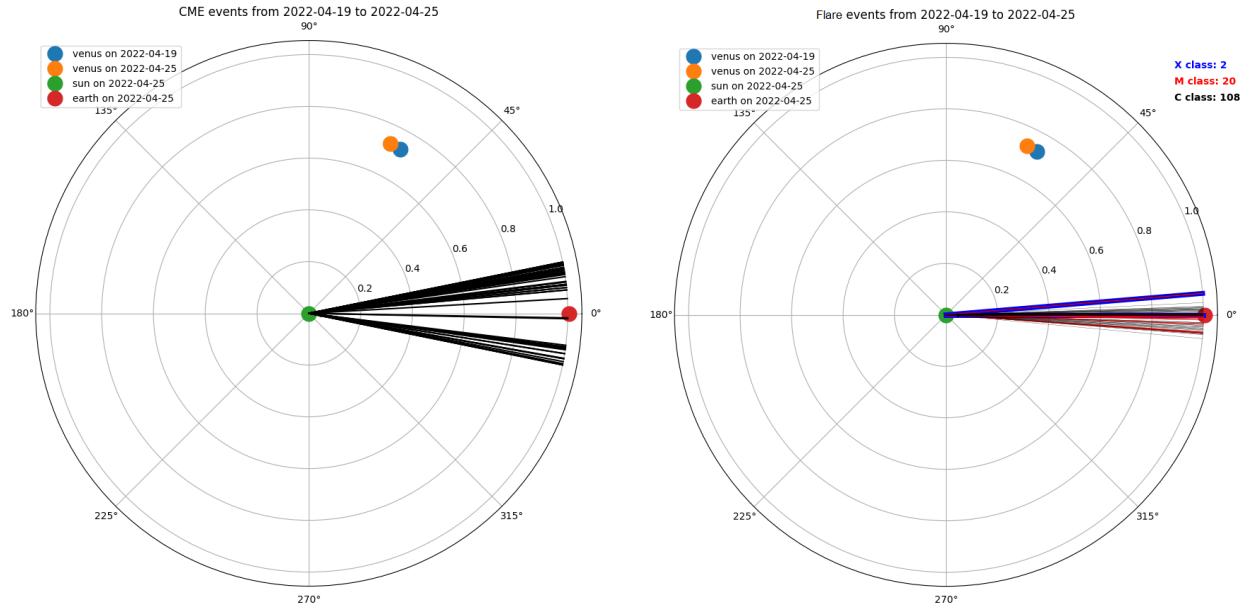


Figure 19: For the 19.04.2022 to 25.04.2022 period: (left) Propagation directions of all CMEs contained in the HEK. (right) Propagation directions of all flares contained in the HEK. The classes of the flares and numbers are indicated in colors.

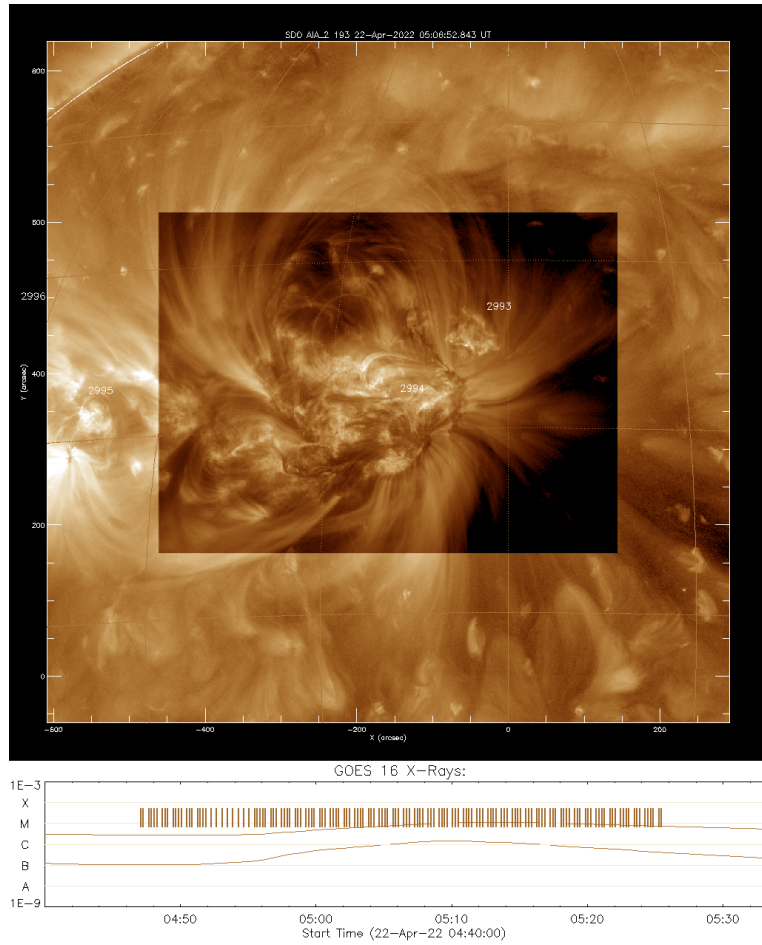


Figure 20: AIA image of the M1.1 class flare visible in the 22.04.2022 window.

Discussion

The fluxes retrieved from Venus' position all show similar averages. The PSF modelling is however the better way to retrieve Venus' flux as it is a somewhat punctual source with very limited extent in the image given its apparent size and the detector's resolution. The question still arises though whether the non-constant or constant model is the best one. Since the solar flux is the main influencer of the X-ray emission of the planet and since it varies on the time scale of minutes, the non-constant model would appear to be the best one especially in high activity periods of the Sun.

Compared to [6], the order of magnitude of the flux found is the same. However, the expected behaviour would be a decrease in the average flux and not an increase as Fig. 16 suggests. The *Dennerl* paper uses only fluorescence as a model and this could be accounted for the discrepancy. The next step of the analysis reported here would be to put thresholds on the different possible emission processes such as charge exchange which was modelled for the Venus atmosphere in [9].

The KS tests performed on the vertical distributions of the fluxes all reject the idea of a direct correlation between the solar flux variability and Venus' although it is less clear for the 24.04.2022 window(4.8%). This is the same conclusion that arised from [6] and the same explanation can be made: Venus was seeing another portion of the Sun and the solar flux variability detected were localised and didn't necessarily impact Venus. The number of points is low though and increasing the statistics would be the next step.

The events are all directed towards Earth and shows the FoV limitation of LASCO and GOES to Earth directed events only. Venus sees a rotated side of the Sun by about $\sim 45^\circ$. But the number of events (54 CMEs and 130 flares $\geq C$) detected in the time interval from the 19.04.2022 to the 24.04.2022 is high. There are therefore no reason to think that the Sun's activity wasn't as high on the Venus' directed side. The fluxes retrieved here should only be used as general indicators of the Sun's activity not as general events directly impacting Venus although the events, in particular the most powerful ones, often have spatial extents of 180° and therefore impacting both planets at the same time. Locating the direction of events not directed towards Earth requires either an X-ray spacecraft to be orbiting the Sun at the desired position or using other methods such as triangulation [10] with the STEREO spacecrafts in heliocentric orbit. This was out of the scope of this project and not explored. The [6] study had the same trouble as they used the GOES missions solar flux data.

Conclusion

In the soft X-ray domain explored by Chandra, Venus was a clear source. In a harder domain (3 keV - 10 keV), this is less obvious with the data presented here. Many differences exist between both analyses, physical and data wise. First of all, Venus doesn't have strong fluorescent scattering in a > 3 keV energy range because these fluorescence mainly concern heavier elements that are only present in the Venusian atmosphere as traces⁹. Secondly, Venus was only observed by chance in the *INTEGRAL* data and it moved in the image. The data was therefore of less quality than the one retrieved by the Chandra spacecraft although the observation conditions were almost as optimal given the orbital parameters. However, the average fluxes calculated were all positive at a high significance level which suggest that the observation was not unsuccessful although more analysis should be made to ascertain this statement. Probing these higher energies are also the occasion to explore different emission processes and thresholds should be computed. Indeed, charge exchange interactions between highly charged heavy solar wind ions and atmospheric neutrals is the dominant process for the X-ray emission of comets for which Venus is a giant version[8].

The concordance between the solar and venusian flux showed its limits of applicability because of the lack of information on potential events hitting Venus. The event direction locator using the HEK gives however a good idea of the high number of events hitting the magnetic field deprived planet every single day.

In conclusion, the study of solar system planets in harder X-ray energies presents an interesting avenue for exploration. The extensive data gathered by the *INTEGRAL* satellite over the past 19 years shows promise for conducting further analysis in this field. By delving deeper into this research, we have the potential to gain valuable insights into the behaviour of our neighbouring planets. The available *INTEGRAL* data offers a solid foundation for future studies and encourages us to continue pushing the boundaries of this analysis.

⁹ See <https://physics.nist.gov/PhysRefData/XrayTrans/Html/search.html> for a list of fluorescence scattering energies and [8]

Annex A

This section contains all subsidiary sky plots and relevant data and models used to obtain the results.

22.04 sky plots

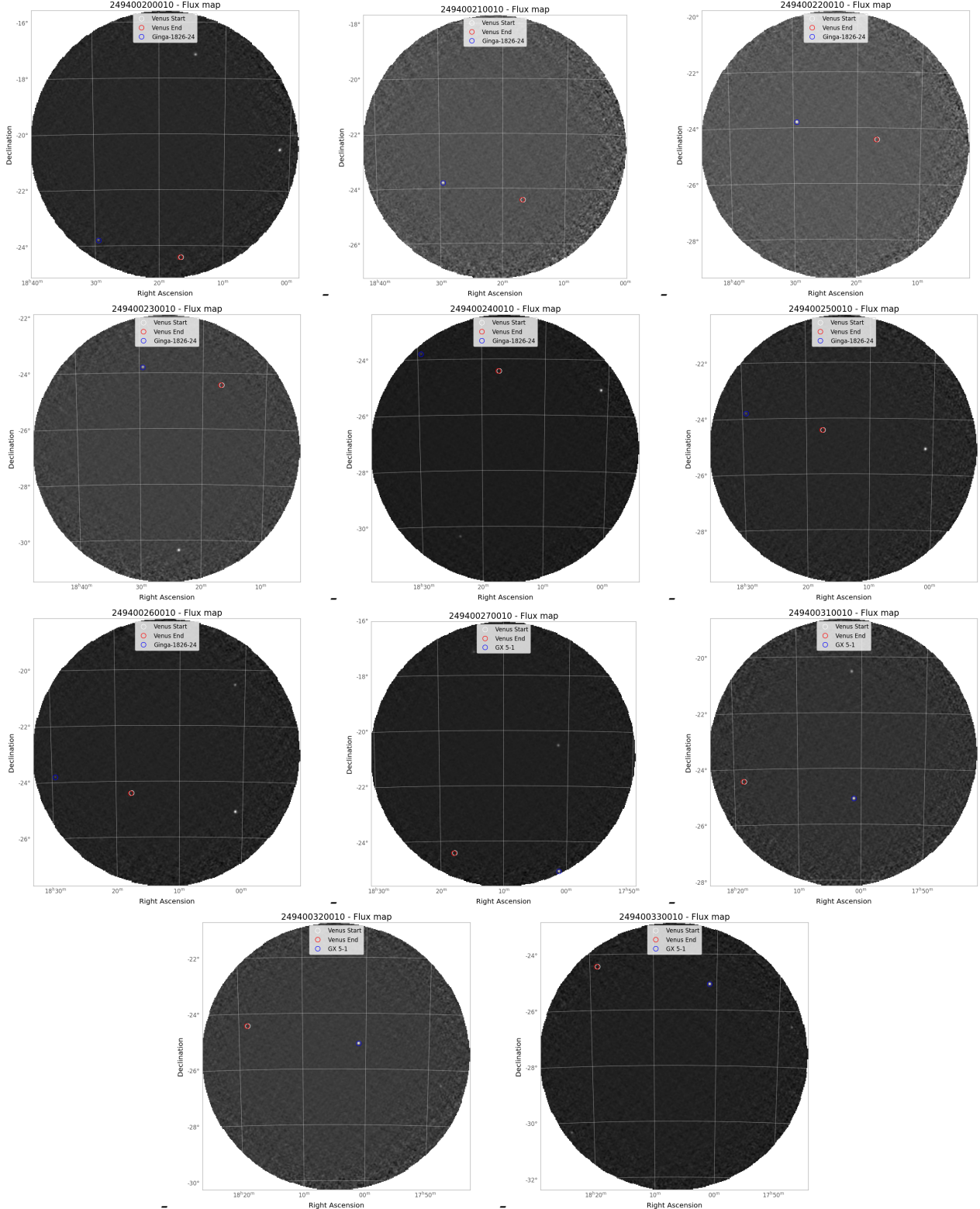


Figure 21: Flux map from every SCW where Venus is present on the 22.04.2022. The start and end positions of Venus are circled in white and red respectively. Another bright source is also to verify the correct localisation approach.

24.04 sky plots

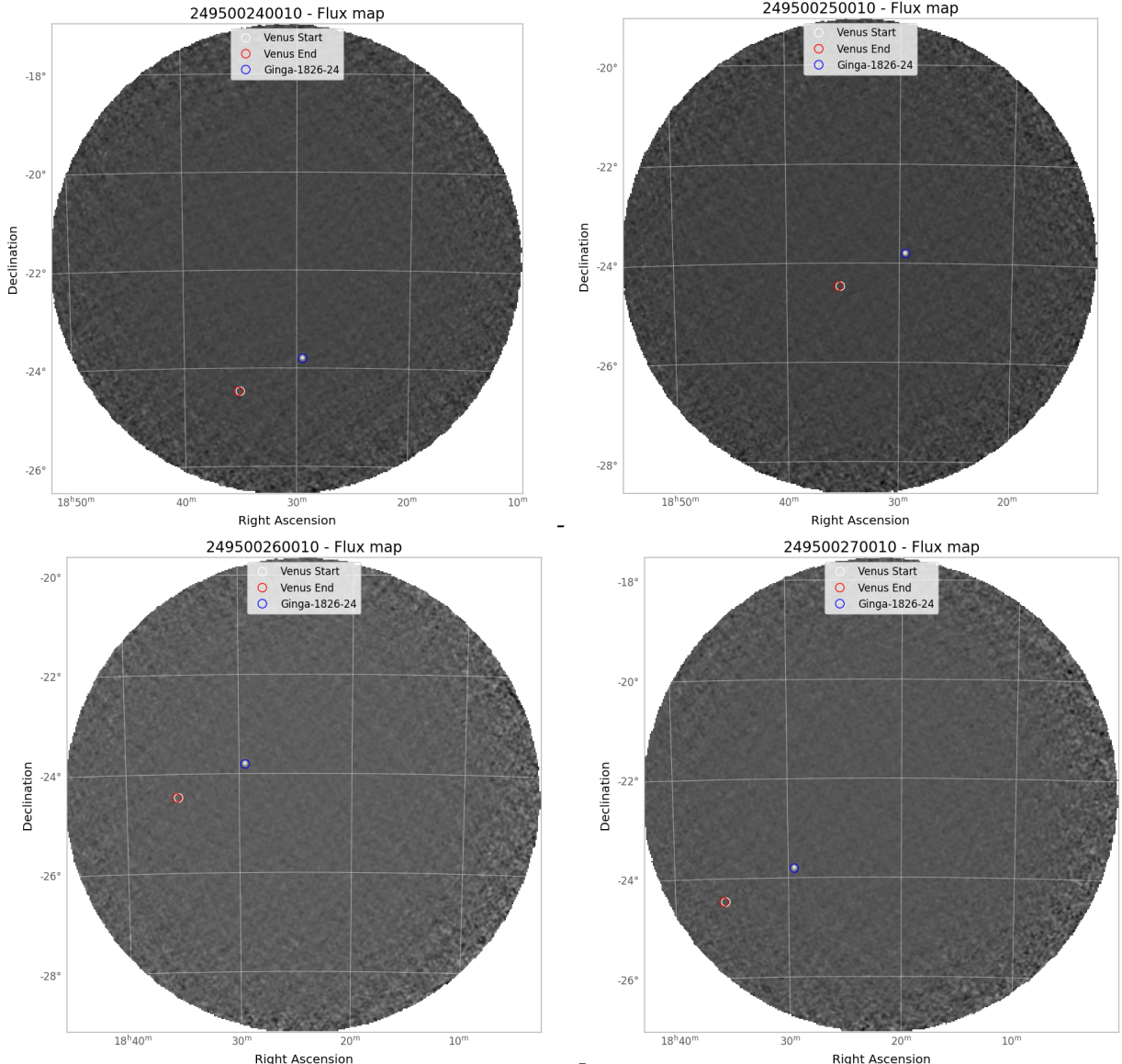


Figure 22: Flux map from every SCW where Venus is present on the 24.04.2022. The start and end positions of Venus are circled in white and red respectively. Another bright source is also to verify the correct localisation approach.

The 2D gaussian models fitted to obtain the different fluxes of Fig. 14 and 15 are the following.

Non constant flux assumption fits

This section shows the different fits and the subsequent model for the non constant flux assumption described in Sec. **Observation, data analysis and methods**.

22.04 data These correspond to the 22.04.2022 data window.

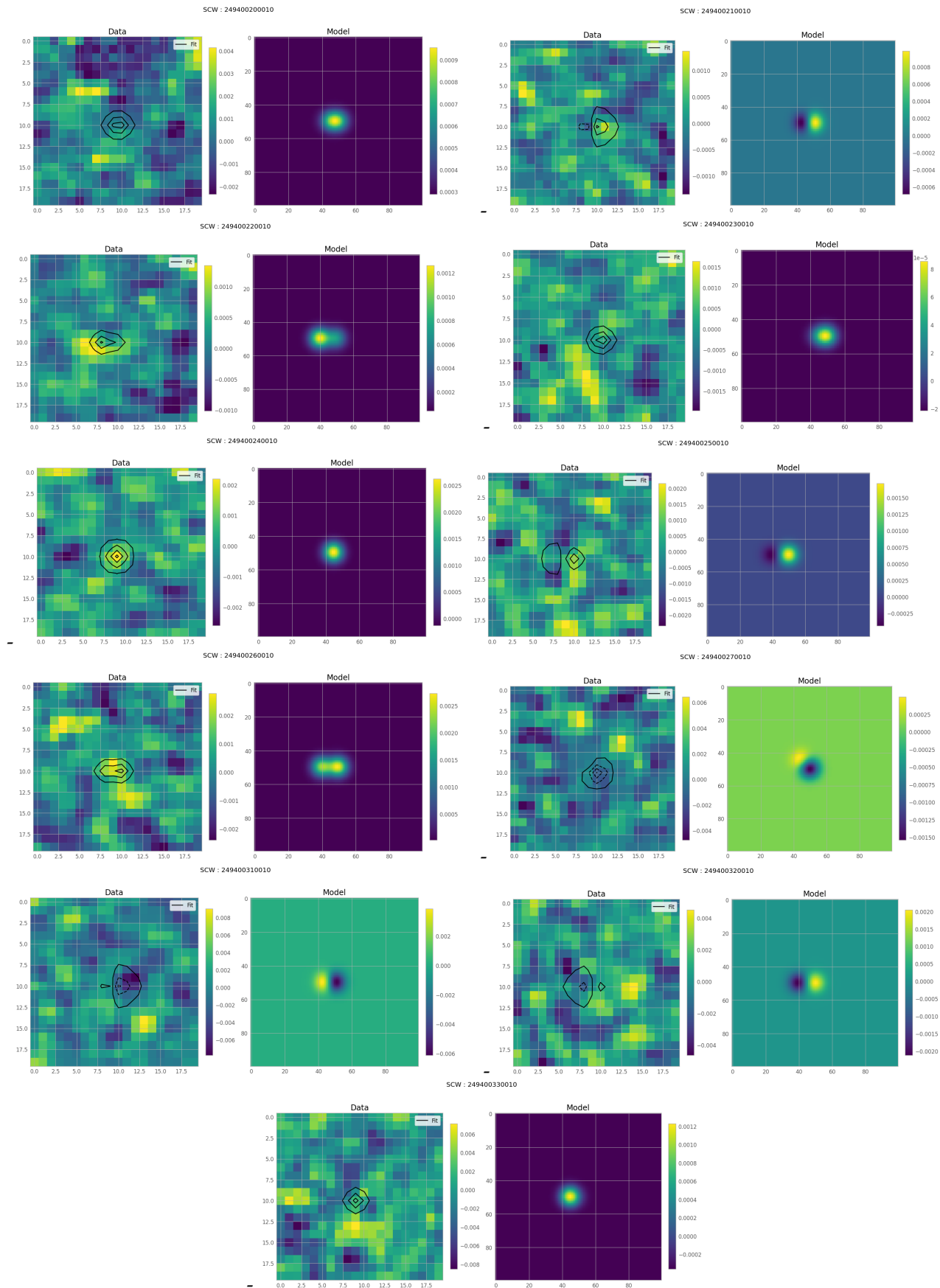


Figure 23

24.04 data These correspond to the 24.04.2022 data window.

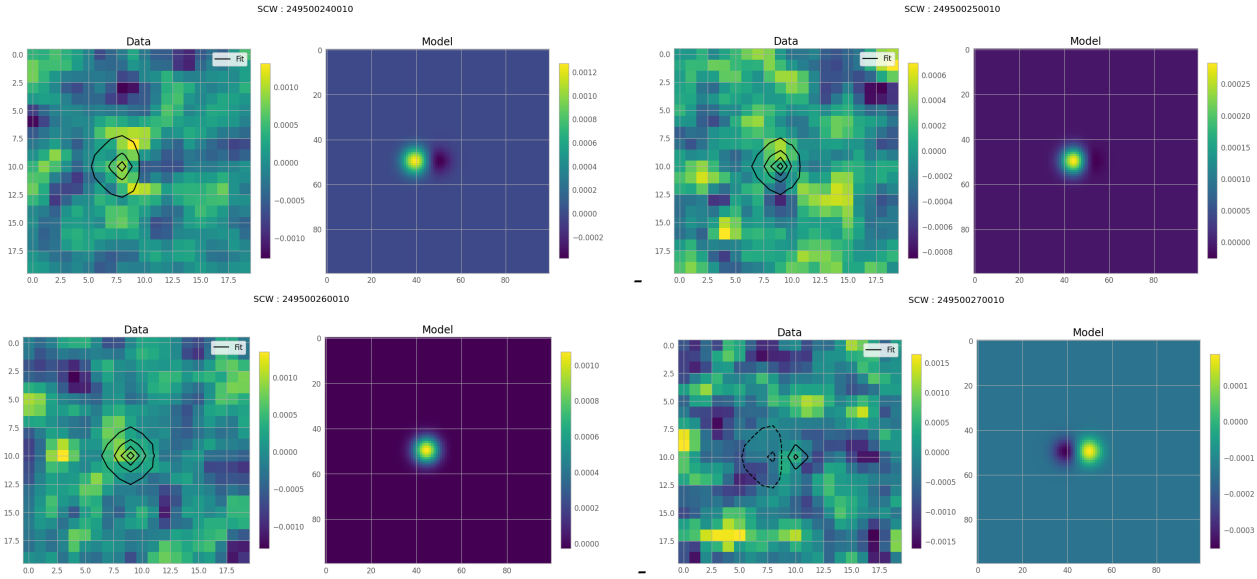


Figure 24

Constant flux assumption fits

This section shows the different fits and the subsequent model for the constant flux assumption described in Sec. Observation, data analysis and methods.

22.04 data These correspond to the 22.04.2022 data window.

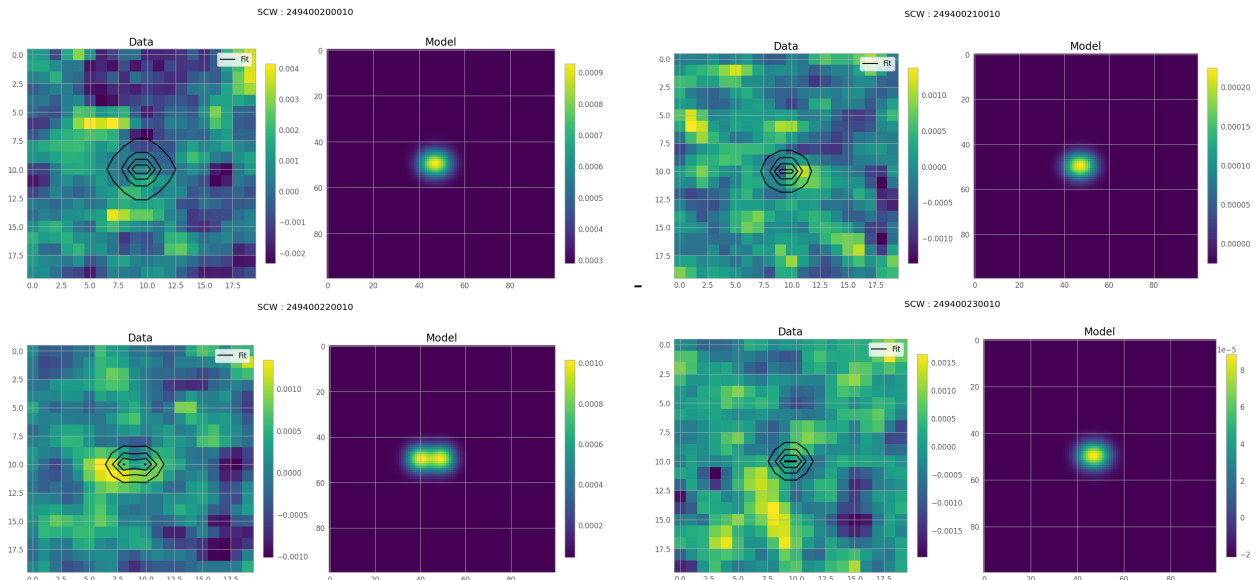


Figure 25

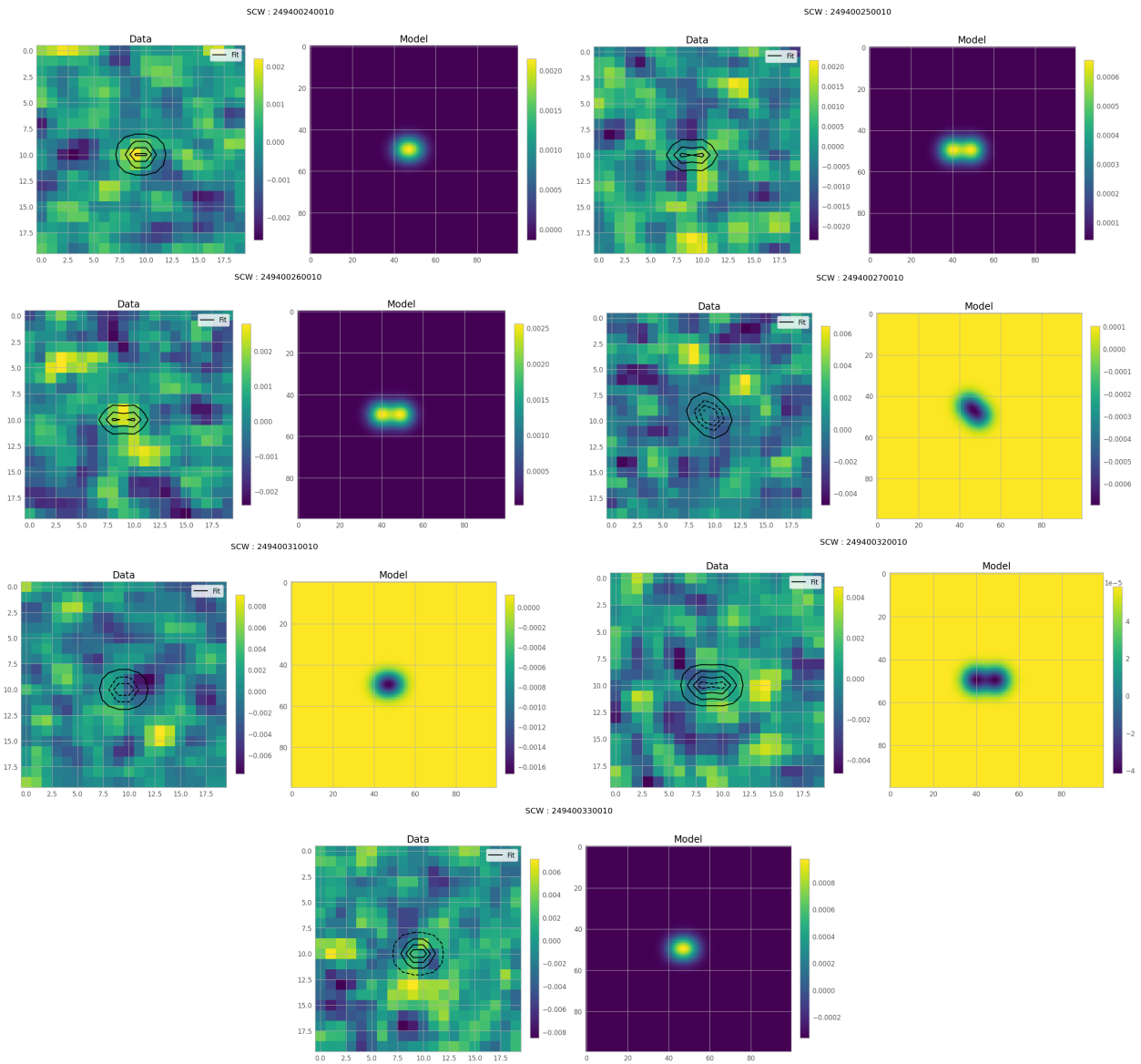


Figure 25 (continued)

24.04 data These correspond to the 24.04.2022 data window.

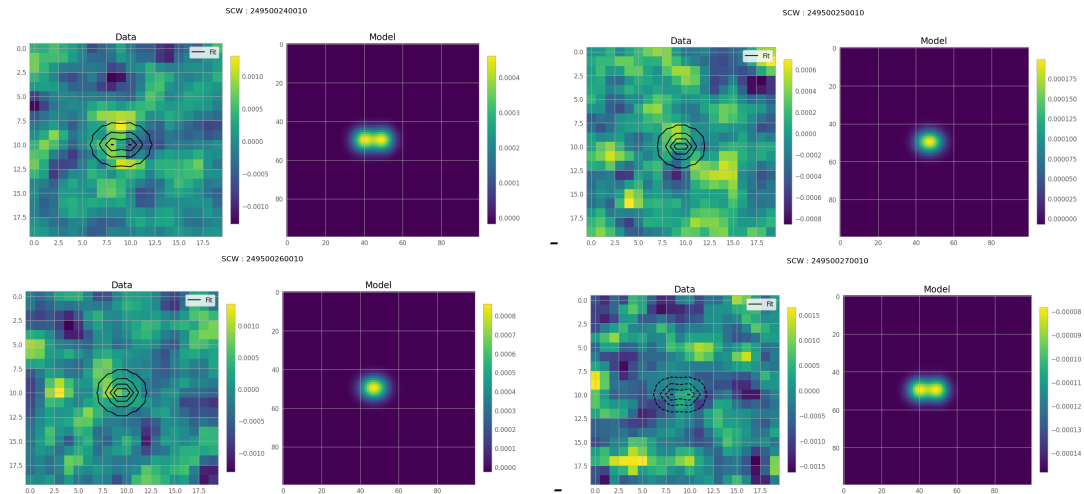


Figure 27

Annex B

The *GitHub* repository corresponding to this project can be accessed here:

<https://github.com/kbarbey/EE-589.git>

Apart from the usual Python libraries, the most important packages used included:

- Sunpy 5.0[11] to access the Heliophysics Event Knowledgebase (HEK) containing the different flare and CME events.
- Skyfield 1.45 to compute ephemerides.
- Astropy 5.2.1

Moreover, the *JPL Horizons* web interface was used to compute the illumination of Venus and its apparent size as seen from the INTEGRAL telescope (observer site code: 500@-198).

References

- [1] https://www.esa.int/Science_Exploration/Space_Science/Integral_overview.
- [2] ISDC JEM-X Analysis User Manual INTEGRAL Science Data Centre JEM-X Analysis User Manual. Tech. rep. 2020. url: <http://isdc.unige.ch>.
- [3] R H Dicke. SCATTER-HOLE CAMERAS FOR X-RAYS AND GAMMA RAYS*. Tech. rep. 1968.
- [4] A. Neronov et al. “An online data analysis system of INTEGRAL telescope”. In: (Feb. 2020). doi: [10.1051/0004-6361/202037850](https://doi.org/10.1051/0004-6361/202037850). URL: <http://arxiv.org/abs/2002.12895%20http://dx.doi.org/10.1051/0004-6361/202037850>.
- [5] Anil Bhardwaj et al. X-rays from Solar System Objects. Tech. rep.
- [6] Ko Dennerl et al. “Discovery of X-rays from Venus with Chandra”. In: *Astronomy and Astrophysics* 386.1 (2002), pp. 319–330. issn: 00046361. doi: [10.1051/0004-6361:20020097](https://doi.org/10.1051/0004-6361:20020097).
- [7] Qi Xu et al. “Observations of the Venus Dramatic Response to an Extremely Strong Interplanetary Coronal Mass Ejection”. In: *The Astrophysical Journal* 876.1 (May 2019), p. 84. issn: 15384357. doi: [10.3847/1538-4357/ab14e1](https://doi.org/10.3847/1538-4357/ab14e1).
- [8] Yoshifumi Futaana et al. Solar Wind Interaction and Impact on the Venus Atmosphere. Nov. 2017. doi: [10.1007/s11214-017-0362-8](https://doi.org/10.1007/s11214-017-0362-8).
- [9] Venus T I Gombosi et al. THE ROLE OF CHARGE EXCHANGE IN THE SOLAR WIND ABSORPTION. Tech. rep. 12. 1981, pp. 126–1268.
- [10] Ying Liu et al. “Geometric Triangulation of Imaging Observations to Track Coronal Mass Ejections Continuously Out to 1 AU”. In: (Jan. 2010). doi: [10.1088/2041-8205/710/1/L82](https://doi.org/10.1088/2041-8205/710/1/L82). URL: <http://arxiv.org/abs/1001.1352%20http://dx.doi.org/10.1088/2041-8205/710/1/L82>.
- [11] Will T. Barnes et al. “The SunPy Project: Open Source Development and Status of the Version 1.0 Core Package”. In: *The Astrophysical Journal* 890.1 (Feb. 2020), p. 68. issn: 0004-637X. doi: [10.3847/1538-4357/ab4f7a](https://doi.org/10.3847/1538-4357/ab4f7a).
- [12] M G F Kirsch et al. *Crab: the standard X-ray candle with all (modern) X-ray satellites*. Tech. rep.
- [13] Celia Sánchez-Fernández. *Science Operations Centre Announcement of Opportunity for Observing Proposals (AO-19) JEM-X Observer’s Manual* INTEGRAL JEM-X Observer’s Manual INTEGRAL JEM-X Observer’s Manual. Tech. rep. 2021.
- [14] J. L. Fox and K. Y. Sung. “Solar activity variations of the Venus thermosphere/ionosphere”. In: *Journal of Geophysical Research: Space Physics* 106.A10 (Oct. 2001), pp. 21305–21335. issn: 21699402. doi: [10.1029/2001ja000069](https://doi.org/10.1029/2001ja000069).
- [15] Janet Machol, Stefan Codrescu, and Courtney Peck. *User’s Guide for GOES-R XRS L2 Products*. Tech. rep. 2023. url: www.ngdc.noaa.gov/stp/satellite/goes-r.html.
- [16] M. Afshari et al. “X-RAYING THE DARK SIDE OF VENUS—SCATTER FROM VENUS’ MAGNETOTAIL?” In: *The Astronomical Journal* 152.4 (Oct. 2016), p. 107. issn: 00046256. doi: [10.3847/0004-6256/152/4/107](https://doi.org/10.3847/0004-6256/152/4/107).